Helix−Helix Association of a Lipid-Bound Amphipathic α-Helix Derived from Apolipoprotein C-II†

Cait E. MacPhee,‡ Geoffrey J. Howlett, William H. Sawyer, and Andrew H. A. Clayton*

Russell Grimwade School of Biochemistry and Molecular Biology, University of Melbourne, Parkville 3052, Victoria, Australia

Received March 29, 1999; Revised Manuscript Received June 4, 1999

ABSTRACT: The interaction of a peptide derived from the sequence of apolipoprotein C-II (apoC-II) with a model lipid surface has been investigated by fluorescence spectroscopy. ApoC-II$_{19-39}$, labeled at the N-terminus with 7-nitrobenz-2-oxa-1,3-diazole (NBD), bound to small unilamellar vesicles of phosphatidylcholine with a dissociation constant of 6 μM. The lipid-bound NBD-labeled peptide exhibited a red-edge excitation shift in its emission maximum and anisotropy, consistent with insertion of the probe into the motionally restricted, polar environment provided by the bilayer interface. The small Stokes shift of the NBD fluorophore permits electronic energy homotransfer between peptides on the lipid surface and results in depolarization of the NBD emission. At high surface densities of lipid-bound peptide, the anisotropy of the NBD probe was 33% lower than in corresponding samples in which electronic energy homotransfer was prevented by the addition of an unlabeled peptide. The efficiency of energy transfer between probes was not consistent with a random distribution of peptides on the lipid surface, indicating instead the self-association of lipid-bound apoC-II$_{19-39}$. We propose that the role of this sequence in apoC-II is not only to mediate binding of protein to a lipid surface, but also to stabilize the lipoprotein complexes by associating with other amphipathic helices within apoC-II and with other apolipoproteins.

Apolipoprotein C-II (apoC-II) is an exchangeable 79-residue apolipoprotein found in blood plasma. In humans, apoC-II is essential for the activation of lipoprotein lipase (LpL) and is therefore important in the hydrolysis of triacylglycerols and the prevention of hypertriglyceridaemia. ApoC-II binds to lipid surfaces with a K_d of 0.4−6.0 μM (*1*, *2*). Structural prediction algorithms suggest that residues 46−52 of apoC-II can form an amphipathic α-helix which may mediate the binding of apoC-II to lipid surfaces (*3*, *4*). Additional evidence for this hypothesis comes from observations that apoC-II$_{44-79}$ binds to a lipid surface and adopts an α-helical conformation (*5*), and that complexes of apoC-II$_{44-79}$ with dimyristoyl phosphatidylcholine vesicles can be isolated by density gradient centrifugation (*6*). A second putative amphipathic α-helix has been identified toward the N-terminus of apoC-II (residues 14−36), but its binding to a phospholipid surface has not been demonstrated (*3*, *4*, *5*). In this paper, we examine the binding of apoC-II$_{19-39}$ to unilamellar phosphatidylcholine vesicles and direct attention to the possibility that the peptide self-associates on the lipid surface.

Association of amphipathic helices may be important in stabilizing the structure of apolipoproteins on the surface of plasma lipid particles. Two structures have been proposed for the lipid-bound form of apolipoprotein A-I (apoA-I). In the first, antiparallel amphipathic helices are oriented parallel to the acyl chains of the phospholipids and stabilize the edge of a bilayer disk (*7*). In a second model, the helix axes within a dimeric apoA-I lie perpendicular to the acyl chains of the phospholipids and form a ring around the bilayer disk (*8*). Although fundamentally different, both models predict that adjacent amphipathic helices are stabilised by interhelical contacts, and that these interactions contribute to the stability of the respective structures.

This raises the question as to whether isolated amphipathic helices are capable of forming similar interhelical contacts, thereby self-associating on the lipid surface. Two lines of evidence indirectly support this postulate. First, the observation that various synthetic amphipathic peptides disrupt phospholipid vesicles to form discoidal micelles is taken as evidence for peptide−peptide interactions at the lipid surface. Second, Spuhler et al. (*9*) studied the binding to a lipid surface of a model peptide derived from the sequence of apoA-I. The binding isotherm could not be explained by the simple partitioning of a monomer into a lipid phase. Inclusion of a positively cooperative peptide−peptide interaction step was necessary to explain the experimental data. This study provided indirect evidence for the formation of interhelical interactions in class A amphipathic peptide−lipid complexes. However, direct physical evidence for the self-association of the peptide on the lipid surface is lacking.

The examination of the self-association of peptides and proteins on or within a lipid bilayer is not trivial. Photoac-

† Supported by a grant from the Australian Research Council. C.E.M. is a recipient of an Australian Postgraduate Research Award. A.H.A.C. is a postdoctoral fellow of the Australian Research Council.

‡ Present Address: Oxford Centre for Molecular Sciences, New Chemistry Laboratory, University of Oxford, South Parks Rd, Oxford OX1 3QT, United Kingdom.

* To whom correspondence should be addressed. Telephone: +613 93447964. E-mail: a.clayton@biochemistry.unimelb.edu.au.

[1] Abbreviations: NBD, 7-nitrobenz-2-oxa-1,3-diazole; apoC-II, apolipoprotein C-II; LPL, lipoprotein lipase; apoA-I, apolipoprotein A-I; homo-EET, electronic energy homotransfer; EYPC, egg yolk phosphatidyl choline; SUVs, small unilamellar vesicles.

10.1021/bi990726b CCC: $18.00
Published on Web 07/30/1999

tivated chemical cross-linking may provide a snapshot of the disposition of peptides at any point in time, and the decay of anisotropy of phosphorescently labeled peptides can potentially provide evidence of changes in the rotational dynamics of peptides on the bilayer surface. A number of studies have used fluorescence resonance energy transfer to measure the association of proteins on lipid surfaces. This technique relies on the strong distance-dependence of the transfer event to elucidate the aggregation state of fluorescently labeled lipid-bound proteins. Such studies include the examination of the aggregation of a MHC Class I protein HLA-A2 (*10*), cation-induced aggregation of the EGF receptor (*11*), and temperature-induced dissociation of the sarcoplasmic reticulum calcium ATPase (*12*). Electronic energy transfer is also useful for the study of peptide self-association in lipid membranes and has been used to study pore formation by pardaxin (*13*), Bti toxin (*14*), and delta endotoxin (*15*). "Donor"- and "acceptor"-labeled peptide analogues have also been used to examine channel formation by the S4 segment of the sodium channel (*16*), the putative transmembrane domain of the minK potassium channel (*17*), and segments of the Shaker potassium channel (*18*). This technique has also provided evidence for the role of the carboxyl terminal regions of potassium channels in dictating pore specificity (*19*).

The above studies have commonly measured the efficiency of transfer between two populations of polypeptides, one labeled with a donor fluorophore, the other with an appropriate acceptor. In contrast, electronic energy homotransfer (homo-EET) examines the transfer of energy between individual peptides or proteins labeled with a single fluorescent probe species. The excitation of a population of probes with polarized light selects those molecules with absorption vectors parallel to the electronic vector of the incident beam. An energy transfer event between these oriented molecules and a neighbor gives rise to depolarization of the emitted light. Runnels and Scarlata (*20*) examined the self-association of melittin in a lipid bilayer using the transfer of energy between fluorescein-labeled monomers. Erijman and Weber (*21, 22*) utilized homo-EET to examine the pressure-induced dissociation of a series of oligomeric proteins. Similarly, Hamman et al. (*23*) used homo-EET between fluorescein-labeled subunits to examine the dimer−monomer dissociation of the *E. coli* ribosomal protein L7−L12 and the kinetics of its subunit exchange.

In this paper, we describe the use of steady-state and time-resolved fluorescence spectroscopy to characterize the interaction of NBD-labeled apoC-II$_{19-39}$ with a model membrane surface. Homo-EET between labeled monomers is used to examine the self-association of this peptide on a lipid surface. We speculate that the role of this sequence is to stabilize the lipid-bound protein through the formation of interhelical interactions within apo-C-II and with other lipid-bound apolipoproteins as well as to mediate the binding of apoC-II to a lipid surface.

MATERIALS AND METHODS

Materials. ApoC-II$_{19-39}$, fully protected at all side-chains and deprotected at the α-amino group of the N-terminal lysine, was purchased from Chiron Mimotopes. The peptide was obtained still attached by its C-terminus to its synthesis "pin". 4-Fluoro-7-nitrobenz-2-oxa-1,3-diazole (NBD) was purchased from Molecular Probes Inc. (Oregan, U.S.A.). Egg yolk phosphatidylcholine (EYPC) was purchased from Lipid Products (Surrey, U.K.). All other reagents were of analytical grade.

N-Terminal Labeling and Purification of ApoC-II$_{19-39}$. ApoC-II$_{19-39}$, (KESLSSYWESAKTAAQDLYEK−NH$_2$) amidated at the C-terminus and attached to the synthesis "pin" was incubated in 99.9% anhydrous dimethylformamide containing a 14-fold molar excess of NBD for 24 h in the dark to specifically label the N-terminal amino group. The pin was washed with dichloromethane, the peptide was cleaved from the pin, and the side-chains were deprotected by immersion in stirred 95% trifluoroacetic acid/2.5% ethanedithiol/2.5% H_2O, (1.5 h at r. t.). The trifluoroacetic acid was removed under N_2, and the peptide was precipitated with ice-cold ether. The cleaved peptide was resuspended in water and lyophilised 3× to remove remaining traces of volatile acid.

Unlabeled apoC-II$_{19-39}$ (1 mmol unmodified) was also prepared, in which case its N-terminal α-amino group was acetylated by reaction for 12 h in acetic anhydride (1 mmol)/dicyclo-hexylcarbodiimide (1 mmol)/N-hydroxybenzotriazole(1 mmol)/di-methylformamide(2 mL) while the peptide was attached to the synthesis pin. The resin-bound peptide was cleaved from the synthesis pin and deprotected as described above.

Crude apoC-II$_{19-39}$ was purified on a semipreparative reverse phase C-18 HPLC column (Brownlee, 10 × 250 mm) using a linear gradient of 20−40% (0.5%/min) acetonitrile containing 0.1% trifluoroacetic acid for elution. Fractions were analyzed by MALDI-TOF mass spectrometry and fluorescence spectroscopy, and the desired fractions pooled and lyophilised 3× from water. The peptide was greater than 95% pure as judged by HPLC using an analytical reverse phase C-18 column (Brownlee Spheri-5, 4.6 × 220 mm) with gradient elution as above.

Preparation of EYPC Unilamellar Vesicles. EYPC was dried to a thin film under a stream of nitrogen and left under vacuum overnight to remove residual traces of organic solvent. Small unilamellar vesicles (SUVs) were prepared in 0.1 M KF, 20 mM Tris, pH 7.4. The suspension was sonicated at 20 kHz in an MSE Soniprep instrument for 15 min under a constant stream of nitrogen. An ice-water bath was used to maintain the temperature of the lipid solution at 20 °C. After sonication, the vesicles were centrifuged to remove residual titanium. Peptide was incubated with SUVs at 30 °C for 12 h, to ensure equilibration prior to fluorescence measurements. The light scattering behavior of vesicles incubated in the presence of peptide was identical to that of a control sample, indicating there were no substantial structural changes in the lipid particle (i.e., vesicle lysis, micellization, or fusion) on peptide binding.

Fluorescence Measurements. Fluorescence measurements were carried out using a SPEX Fluorolog/Tau-2 spectrofluorometer using a 5 mm path-length cuvette. For steady-state measurements, excitation of the NBD-labeled peptide was at 455 nm; emission spectra were measured in the wavelength range 480−650 nm. Excitation and emission slit widths were 5 nm. Background due to scattered light was subtracted using an appropriate unlabeled control. The fluorescence lifetime of NBD was measured in the frequency

domain against a fluorescein standard (lifetime of 4.05 ns) using 20 frequencies in the range of 5−200 MHz. The phase angle and modulation values obtained at each frequency were the average of 5 measurements, acquired over a 30 s integration time. Excitation of the NBD fluorophore was accomplished using vertically polarized, 455 nm excitation from a Xe lamp. The fluorescence was observed at 550 nm after being passed through a polarizer oriented at the magic angle (55°). The frequency domain data were analyzed using Globals Unlimited software (University of Illinois, Urbana-Champaign), employing a sum of discrete exponentials to model the data. The goodness-of-fit was assessed by the value of χ^2.

Fluorescence Depolarization Resulting from Energy Homotransfer. Fluorophores with small Stokes shifts can undergo energy self-transfer, which is detected by depolarization of the fluorescence emission (*24*). The efficiency of energy transfer (E) can be calculated from the steady-state anisotropy in the absence and presence of energy transfer assuming an orientation factor (κ^2) of 2/3, which describes the condition of rapid reorientation of donors and acceptors within the fluorescence lifetime (*23*):

$$E = \frac{2(r_{01} - \langle r \rangle)}{r_{01}} \quad (1)$$

where $\langle r \rangle$ is the observed anisotropy and r_{01} is the anisotropy in the absence of energy transfer. The fluorescence quantum yield (Q) of NBD-labeled peptide in the presence and absence of excess lipid was determined relative to a 90 nM stock solution of fluorescein in 0.01 M NaOH ($Q = 0.93$). The overlap integral (J) was determined from the overlap between the absorption spectrum, in units of M^{-1} cm^{-1}, and the corrected emission spectrum as:

$$J = \frac{\int F_d(\lambda)\epsilon(\lambda)\lambda^4 d\lambda}{\int F_d(\lambda) d\lambda} \quad (2)$$

where $F_d(\lambda)$ and $\epsilon(\lambda)$ are the fluorescence emission and the molar absorption coefficient, respectively, at wavelength λ. The Förster critical distance (R_0) in angstroms over which energy transfer between fluorophores is 50% efficient, was calculated from:

$$R_0 = 9.78 \times 10^3 (Q_D \kappa^2 n^{-4} J)^{1/6} \quad (3)$$

where Q_D is the quantum yield of donor in the absence of energy transfer, and n is the refractive index of the medium (1.4).

RESULTS

Lipid-Binding of NBD-Labeled ApoC-II$_{19-39}$ and Its Transverse Location in the Bilayer. The absorption and fluorescence spectra of the NBD-labeled peptide in aqueous solution are presented in Figure 1. The absorption spectrum is typical of NBD in aqueous solution. The lowest energy $S_1 \leftarrow S_0$ transition consists of a single asymmetric band centered at 467 nm with extinction coefficient 15 585 cm^{-1} M^{-1}. The fluorescence spectrum of NBD-labeled peptide displays a Stokes shift of approximately 76 nm (2997 cm^{-1}) and shows a good mirror image relationship with respect to the excitation spectrum.

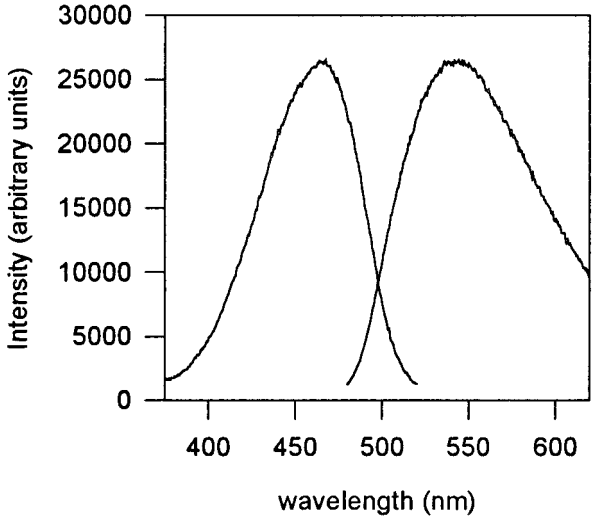

FIGURE 1: Absorption (left) and normalized emission (right) spectra of NBD-apoC-II$_{19-39}$ in aqueous solution.

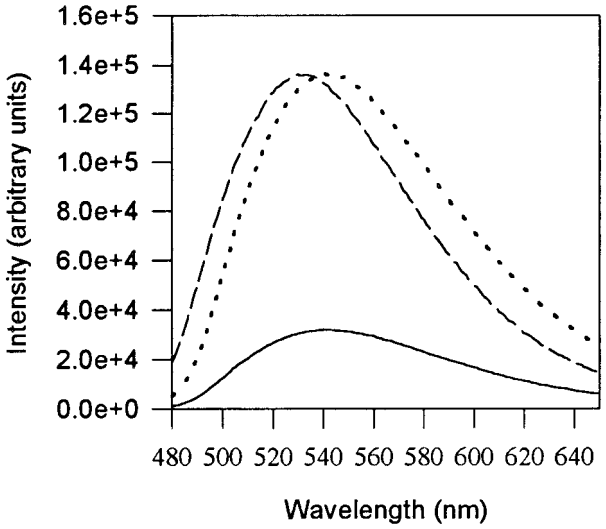

FIGURE 2: Emission spectra of NBD-labeled apoC-II$_{19-39}$ in the presence and absence of EYPC SUVs. The solid line represents 11 μM NBD-apoC-II$_{19-39}$ in aqueous solution. The dashed line represents the same concentration of peptide in the presence of 6 mM EYPC. The dotted line represents the emission spectra of peptide in aqueous solution, normalized to the emission spectrum of the lipid-bound peptide.

The effect of the binding of apoC-II$_{19-39}$ to EYPC SUVs on the fluorescence properties of the NBD fluorophore is shown in Figure 2. There is a 5-fold increase in fluorescence quantum yield from 0.044 to 0.24, coupled with a 13 nm blue shift in the emission maximum from 543 to 530 nm. The increase in fluorescence intensity was used to monitor the interaction of apoC-II$_{19-39}$ with lipid vesicles. Figure 3 shows the normalized increase in fluorescence intensity upon the addition of EYPC SUVs. The solid line represents the fit to a K_d of 6.3 μM, with a stoichiometry of 36 phospholipids per peptide. These values agree well with those obtained previously in this laboratory by quantitative mass spectrometry (5 μM, 35 phospholipids/ peptide) for unlabeled apoC-II$_{19-39}$ in which the NBD label was replaced by acetylation of the N-terminal amino group (MacPhee, Howlett, and Sawyer, unpublished results). These results

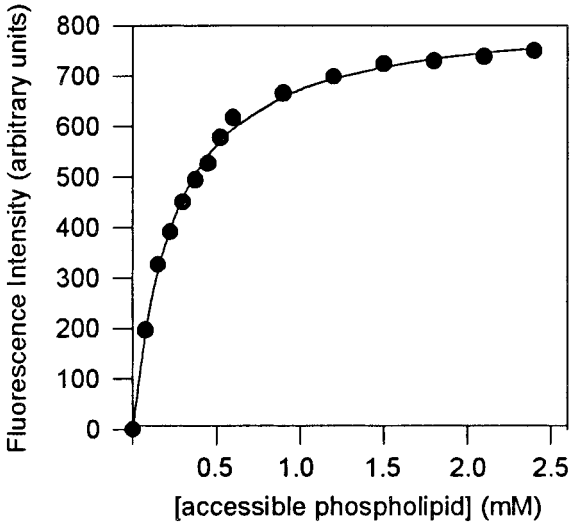

FIGURE 3: Titration of 1.7 μM NBD-apoC-II$_{19-39}$ with EYPC SUVs. The symbols represent the increase in fluorescence intensity (ex 465 nm, em 525 nm) upon the addition of lipid. All samples were incubated for 12 h prior to measurement. The solid line is the nonlinear least-squares fit for a K_d of 6.3 μM and a stoichiometry of 36 phospholipids/peptide.

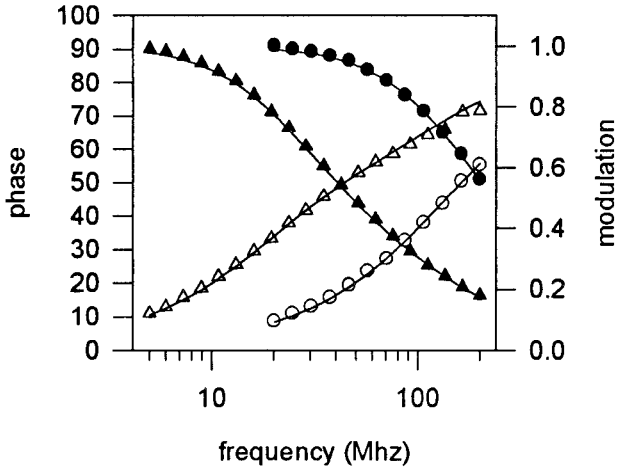

FIGURE 4: Frequency domain lifetime data for 2.15 μM NBD-apoC-II$_{19-39}$ in the presence (triangles) and absence (circles) of 2.5 mM EYPC. Phase angle (open symbols) and modulation frequency (filled symbols) data in the absence of lipid were fitted to a single discrete lifetime of 1.2 ns ($\chi^2 = 2.1$). In the presence of lipid, data were fitted to the population-weighted sum of two discrete lifetimes, 1.8 and 7.1 ns ($\chi^2 = 3.3$).

suggest that labeling of apoC-II$_{19-39}$ with NBD has a minimal effect upon the affinity of the peptide for a lipid surface. An alternative transformation of the data in Figure 3 was also undertaken to generate the conventional binding isotherm described by Seelig and co-workers (*9*). Analysis of the curve yielded a predominantly straight-line (correlation coefficient 0.98) with a partition coefficient of 4.8×10^3 M^{-1} (results not shown).

Similar changes to the NBD fluorescence spectrum have been reported for other NBD-labeled molecules in organic−aqueous solvent mixtures, egg yolk phosphatidylcholine large unilamellar vesicles, and DOPC multilamellar vesicles (*25*, *26*, *27*). The similarity of the fluorescence quantum yield of lipid-bound NBD-apoC-II$_{19-39}$ to that exhibited by *n*-propylamino-NBD in water−organic solvent mixtures suggests that the dielectric constant experienced by the lipid-bound probe is in the range 20−40 (*27*). Although the precise dielectric gradient in the bilayer has been the subject of some debate, this estimate of the local dielectric constant is consistent with localization of the NBD group near the headgroup region of the bilayer (*27*).

Multifrequency domain lifetime measurements also provided a sensitive indicator of the environmental changes experienced by the peptide-conjugated NBD probe on binding to lipid, as seen by the frequency domain plots in Figure 4. The observed shift of the phase and modulation curves to lower frequency on formation of a peptide−lipid complex reflects a larger NBD fluorescence lifetime in the lipid-bound peptide compared with aqueous solution. Analysis of the phase-modulation data revealed a single-exponential decay for the NBD-peptide fluorescence in aqueous solution with a lifetime of 1.2 ns. This lifetime agrees with values of 1.1 ns obtained for other NBD-labeled systems in aqueous solution (*26*). However, in the presence of EYPC SUVs, the fluorescence decay of the NBD-peptide could not be fitted to a single-exponential model ($\chi^2 = 92$). This implies a heterogeneous environment for the NBD probe in the peptide-lipid complex. A biphasic description of the phase-modulation data greatly improved the quality of the fit, the two time constants being 1.8 ns (fractional population 48%) and 7.1 ns (fractional population 52%) ($\chi^2 = 3.3$). The population-weighted average fluorescence lifetime of the NBD-labeled peptide in vesicles was 4.6 ns, a value similar to that obtained for an N−NBD-ethanolamine probe in a 25% water−75% ethanol mixture (4.1 ns; *26*).

Previous photophysical studies of NBD derivatives in solvents of varying dielectric constant have shown that the nonradiative rate constants of excited-state deactivation are particularly sensitive to environment and can provide an estimate of the local polarity of the environment about the NBD fluorophore (*27*). From the quantum yield (Q) and lifetime (τ) values obtained above, it is possible to calculate the nonradiative rate constants (k_{nr}) of deactivation of the NBD excited-state as

$$k_{nr} = (1 - Q)/\tau \qquad (4)$$

For NBD-apoC-II$_{19-39}$ in aqueous solution, the nonradiative rate constant was 7.9×10^8 s^{-1}. This value is consistent with an environment of dielectric constant between 70 and 75 (*27*) and suggests that the NBD fluorophore is largely exposed to the aqueous phase. In the peptide−lipid complex, the average NBD nonradiative rate is reduced to 1.7×10^8 s^{-1}, which correlates with a dielectric constant between 30 and 40 and is consistent with the NBD group being located at the headgroup/interfacial region of the lipid bilayer (*27*). This conclusion from the time-resolved data is, therefore, in agreement with that reached on the basis of the steady-state fluorescence data.

A qualitative measure of environmental heterogeneity and rigidity about the NBD chromophore was provided by red-edge excitation shift spectroscopy (REES), a technique of increasing importance in the characterization of fluorophore-solvent interactions in restricted environments (*28*). In general, a motionally restricted heterogeneous environment causes (1) a dependence of the fluorophore emission maximum on the excitation wavelength, and (2) an increase in the anisotropy of the fluorophore emission at the red-edge of the absorption band due to selection of those

fluorophores forming strong interactions with the solvent and/or selection of fluorophores having a reduced probability of undergoing energy transfer. For the NBD-apoC-II_{19-39} conjugate, these REES effects are observed in both aqueous solution and in the lipid-bound state but are more pronounced in the latter. Thus, for the NBD-peptide bound to SUVs, there is a 25 nm (856 cm^{-1}) shift in the emission maximum on changing the excitation wavelength from 425 to 505, significantly larger than the 9 nm (300 cm^{-1}) shift observed for the NBD-peptide in aqueous solution. Similarly, changing the excitation wavelength from 425 to 505 nm produces an anisotropy shift from 0.18 to 0.23 in the NBD-peptide−lipid complex compared with a shift from 0.07 to 0.08 in aqueous solution. The more pronounced red-edge effect exhibited by NBD-apoCII_{19-39} in the peptide−lipid complex compared to aqueous solution is consistent with insertion of the peptide into a heterogeneous polar environment in which the solvent molecules are motionally restricted. Together with the time-resolved and steady-state fluorescence data, these results indicate that the NBD-peptide is located near the polar-interfacial region of the bilayer where it experiences a heterogeneous environment. This conclusion is substantiated by preliminary tryptophan fluorescence measurements (MacPhee, Howlett, Sawyer, unpublished observations) which show that the emission maximum (336 nm) of the single tryptophan at position 8 in the sequence is consistent with a local environment equivalent to that of the interfacial/headgroup region of the bilayer (*29*). We next turn to the question of the lateral distribution of the peptides on the lipid surface and detection of peptide self-associations using energy homotransfer.

Electronic Energy Homotransfer between Lipid-Associated Peptides. The small Stokes shift exhibited by the fluorophore (Figure 1) raises the possibility of homo-EET between suitably proximal NBD chromophores. The change in spectral properties of the NBD probe on formation of a peptide−lipid complex gives rise to an increase in the value of the Förster spectral overlap integral, from 5.176×10^{-15} M^{-1} cm^3 for peptide in aqueous solution, to 1.053×10^{-14} M^{-1} cm^3 in the presence of SUVs. This results in an increase in the Förster critical distance (R_o) from 18 Å for NBD-labeled apoC-II_{19-39} in solution, to 26 Å for the lipid-bound peptide. These calculations demonstrate that detection of energy transfer between NBD fluorophores on the lipid surface will be possible using steady-state methods, if the separation between NBD-labeled peptides is in the range 13−39 Å.

The steady-state anisotropy of lipid-bound NBD-apoC-II_{19-39} decreases as the surface density of bound peptide increases as shown in Figure 5; the fluorescence undergoes little change in intensity but is increasingly depolarized. The lack of an appreciable intensity change rules out simple quenching or changes in light scattering as major causes of fluorescence depolarization. An alternative cause of an anisotropy decrease could be due to an increase in the NBD fluorescence lifetime with increasing peptide surface density. However, this would result in a concomitant increase in fluorescence intensity—in disagreement with the observed results. At the highest concentration of NBD-apoC-II_{19-39} examined, the fluorescence anisotropy decreased 37%. In contrast, a parallel series of samples containing the same total concentration of peptide, of which only 10% is NBD-labeled, showed only a 4% decrease across the total range of peptide surface densities. We conclude that the 37% decrease in anisotropy is due to homotransfer of electronic energy between the NBD-labeled peptides.

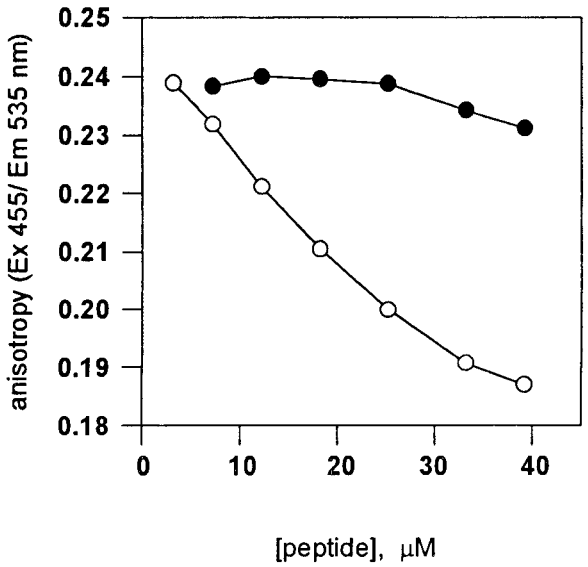

FIGURE 5: Fluorescence anisotropy of NBD-apoC-II_{19-39} in the presence of 4 mM EYPC. The open circles represent data obtained for samples containing 2×10^{-7} to 3.9×10^{-5} M NBD-apoC-II_{19-39}. The filled circles represent data obtained for samples containing a 1:9 ratio of labeled/unlabeled apoC-II_{19-39}, where the total concentration of peptide (labeled + unlabeled) in the sample was 2×10^{-7} to 3.9×10^{-5} M. (ex 455 nm, em 535 nm).

DISCUSSION

Evidence for Peptide Self-Association. Fluorescence depolarization resulting from an increase in the concentration of fluorophores on a membrane surface has been reported previously and modeled theoretically (*10*, *30*). In the present case, the important question is whether the concentration-dependent depolarization shown in Figure 5 is the result of a random distribution of NBD-peptide molecules or the result of high local surface densities of peptide due to peptide self-association. Theory can predict the correct form of the depolarization dependence for a random distribution of fluorophores on the bilayer surface. A comparison of this dependence with that observed from experiment provides a means of assessing the association state of the peptide.

Our approach to the problem follows the work of Wolber and Hudson (*31*) that predicts the energy transfer efficiencies for heterotransfer between donor and acceptors randomly distributed on a two-dimensional surface as a function of fluorophore surface density. There are three conditions of this theory for donor−acceptor heterotransfer that need to be addressed in the case of donor−donor homotransfer: (1) the concentration of excited donors must be less than the concentration of acceptors to ensure that the measured transfer efficiency corresponds to a single transfer from excited donor to acceptor. For the present case of identical donor and acceptors, the corresponding assumption is that the fluorescence anisotropy is primarily determined by the initially excited donor molecule and that a single transfer event is sufficient to cause complete depolarization of the light emitted from the acceptor. We note that even if this assumption does not hold then the measured transfer ef-

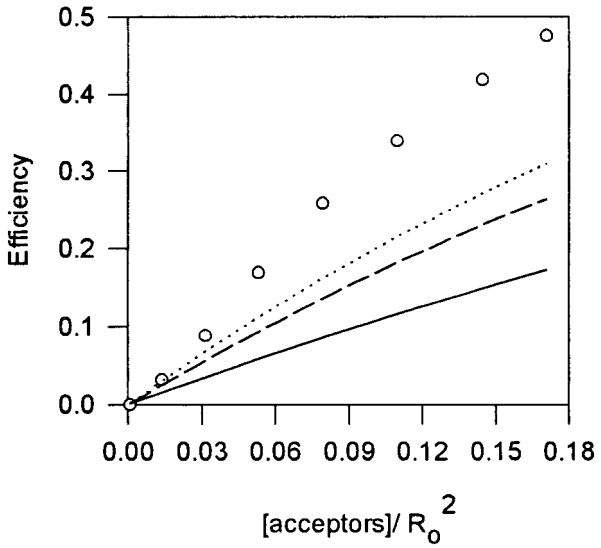

FIGURE 6: The efficiency of energy transfer between NBD-apoC-II$_{19-39}$ plotted as a function of peptide surface-binding density, the surface density expressed as [NBD-peptide]/R_0^2. The open circles represent the experimental data, derived from Figure 5. The lines represent the predicted efficiency of energy transfer between fluorophores attached to a rigidly extended peptide with Stokes radius of 15 Å (solid line), a randomly coiled peptide of Stokes radius 11.7 Å (dashed line), and an α-helical peptide of Stokes radius 10.3 Å (dotted line).

ficiency will provide a lower bound of the single-step energy transfer efficiency between proximal donor molecules; (2) a random orientational distribution of donor and acceptors is assumed. Since we have no detailed information on the orientational distribution of the NBD probe, we will retain this assumption as a first approximation; (3) the distance of closest approach (R_e) between donor and acceptor is less than the Förster critical transfer distance (R_o). This condition will be shown to be valid below.

The transfer efficiency depends on three variables: the surface density of the fluorophores, the critical transfer distance (R_0), and the distance of closest approach between the donor−acceptor pair (R_e). The ratio R_e/R_0 is an important dimensionless variable, and its value determines the magnitude and functional form of the energy transfer efficiency with fluorophore surface concentration. We have evaluated the energy transfer efficiency from the anisotropy data (eq 1) and calculated the average surface density from the known number of peptides per vesicle and the vesicle surface area. The surface density is expressed as the concentration of fluorophores within an area described by the Förster critical distance (R_0^2). The experimentally derived transfer efficiency-surface density profile is shown in Figure 6 (*hollow circles*).

For comparison, the efficiency of energy transfer (E) between monomeric fluorophores randomly distributed and oriented on a planar surface, as a function of surface density (c) has been calculated from the formula of Wolber and Hudson (*31*),

$$E = 1 - (A_1\exp(-k_1c) + A_2\exp(-k_2c)) \qquad (5)$$

where the parameters A_1, A_2, k_1, and k_2 are constants that depend on the ratio R_e/R_0 (given in Table 1 of Wolber and Hudson (*31*)). The Förster critical transfer distance (R_o) and the values of c are determined from experiment and fixed, while the distance of closest approach (R_e) is dependent on the structure of the peptide on the lipid surface. As the structure of apoC-II$_{19-39}$ on a lipid surface is not known, three different conformational states were modeled to give estimates for R_e. The first conformation modeled assumed that the Stokes radius for the lipid-bound peptide corresponded to that for apoC-II$_{19-39}$ in aqueous solution, as measured by analytical ultracentrifugation (*32*). This value of the Stokes radius gave a distance of closest approach of 20.7 Å or ca. $0.8R_o$. This is an unrealistic approximation for the lipid-bound form of the peptide since circular dichroism measurements show that the peptide exists as a random coil in solution but as an α-helix in the peptide−lipid complex (MacPhee, Howlett, and Sawyer, unpublished results). Nevertheless, the maximum efficiency of energy transfer between peptides randomly distributed on a lipid surface at the highest surface density of peptide was predicted to be 26% (Figure 6, dashed line).

The second conformation assumes that the peptide exists on the lipid surface as an ideal 21-residue α-helical peptide. There is no unraveling of the helix ends or helical motion. The structure of the helix was generated using the software package Hyperchem (Hypercube Inc.). A Stokes radius of 15 Å was computed using the bead model of the α-helix provided by Byron (*33*) and provided a value of 26.6 Å for R_e. At the highest surface density of lipid-bound peptide examined, this conformation would lead to a 15% efficiency of energy transfer (Figure 6, solid line).

The third conformation modeled for the lipid-bound peptide was derived from data acquired for an unrelated but monomeric α-helical 21-residue peptide in TFE (*34*). The Stokes radius determined by analytical ultracentrifugation was 10.3 Å, corresponding to a value for R_e of 18.3 Å, or $0.7R_o$. The maximum predicted transfer efficiency between peptides in this conformation at the highest surface density measured is about 30% (Figure 6, dotted line).

In each case, the predicted energy transfer efficiency does not approach that of lipid-bound NBD-labeled apoC-II$_{19-39}$ found by experiment (Figure 6, open circles). The experimental data could be fitted to a random distribution of peptides if R_0 was taken to be 52 Å. However, such a high value is not compatible with that obtained from spectral data and would require large and theoretically impossible values for the orientation factor. Thus, a model involving randomly distribution of monomers on the lipid surface cannot account for the observed efficiencies of homotransfer within the range of peptide surface densities examined. We, therefore, conclude that the high-transfer efficiencies are the result of self-association of the peptides on the lipid surface.

Relevance to Lipoprotein Structure. The ability of apoC-II$_{19-39}$ to self-associate on a lipid surface may reflect a common property of lipid-bound amphipathic α-helices. Palgunachari et al. examined the ability of the eight putative class A helices from the sequence of apoA-I to interact with a lipid surface (*35*). Despite the common class A status, only two helices were found to interact significantly with lipid. The authors hypothesized that these were responsible for the initial tethering of the protein to the lipid surface, to be followed by a cooperative conformational change in one or more of the remaining amphipathic helices. The final antiparallel array of helices at the lipid−water interface was then stabilized by interhelical ionic and hydrophobic interactions. Lins et al. (*36*) and Phillips et al. (*7*) used a molecular

modeling and energy minimization approach to explore the possibility that interhelical ionic interactions and salt-bridge formation between adjacent class A helices stabilized the lipid-bound form of apoA-I. The authors suggest that the major contribution to stability arises from hydrophobic interactions between nonpolar residues and the hydrophobic acyl chain region of the lipid bilayer. However, additional stability is derived from interactions between polar residues and water at the bilayer interface and salt bridge formation between side-chains of complementary charge.

Similarly, of the four amphipathic helices predicted within the sequence 202−286 of apolipoprotein E (*4*), only one peptide containing residues 263−286 bound significantly to lipid (*37*). Lins et al. (*36*) suggest that the binding of apoE to lipid surfaces may also be mediated by cooperative interhelical interactions between a lipid tethering helix (residues 262−286) and the three putative amphipathic helices between residues 202−263. Alternatively, the helix between residues 263−286 may interact at a lipid surface with a previously identified lipid-binding helix between residues 129−169 (*38*).

Besides stabilizing helices within apolipoproteins, association of amphipathic helices may also occur between different apolipoprotein molecules. Interactions between apolipoprotein classes may explain the observed modulatory effects of some apolipoproteins on apoC-II. For example, the amphipathic α-helical lipid-binding region of apoC-III is known to inhibit apoC-II-mediated activation of lipoprotein lipase (*39*, *40*, *41*). This inhibition is thought to be due to the binding of apoC-III directly to LpL (*42*), although formation of an LpL-apoC-III complex could not be demonstrated (*43*). We suggest that the modulatory actions of apoC-III may arise through the formation of inter-apolipoprotein interactions between the amphipathic, lipid-binding regions of apoC-III and apoC-II. Thus, the lipid-induced homologous association of apoC-II_{19-39} described in this paper may be illustrative of a heterologous association that occurs within and between apolipoproteins in general.

REFERENCES

1. McLean, L. R., and Jackson, R. L. (1985) *Biochemistry 24*, 4196−4201.
2. Posner, I. (1982) *Atheroscler Rev 9*, 123−156.
3. Mantulin, W. W., Rohde, M. F., Gotto, A. M. Jr, and Pownall, H. J. (1980) *J. Biol. Chem. 255*, 8185−8191.
4. Segrest J. P., Jones M. K., De Loof H., Brouillette, C. G., Venkatachalapathi, Y. V., and, Anantharamaiah, G. M. (1992) *J Lipid Res 33*, 141−166.
5. Sparrow, J. T., and Gotto, A. M. (1980) *Ann. NY. Acad. Sci. 348*, 187−211.
6. Smith, L. C., Voyta, J. C., Catapano, A. L., Kinnuna, P. K., Gotto, A. M., and Sparrow, J. T. (1980) *Ann. NY. Acad. Sci. 348*, 213−223.
7. Phillips, J. C., Wriggers, W., Li, Z., Jonas, A., and Schulten, K. (1997) *Biophys. J. 73*, 2337−2346.
8. Borhani, D. W., Rogers, D. P., Engler, J. A., and Brouillette, C. G. (1997) *Proc. Natl. Acad. Sci. U.S.A. 94*, 12291−12296.
9. Spuhler, P., Anantharamaiah, G. M., Segrest, J. P, and Seelig, J. P. (1994) *J Biol Chem 269*, 23904−23910.
10. Chakrabarti, A., Matko J., Rahman, N. A., Barisas, B. G, and Edidin, M. (1992) *Biochemistry 31*, 7182−7189.
11. Carraway, K. L., Koland, J. G., and Cerione, R. A. (1989) *J. Biol. Chem 264*, 8699−8707.
12. Fagan, M. H., and Dewey, T. G. (1986) *J. Biol. Chem 61*, 3654−3660.
13. Rapaport, D., and Shai, Y. (1992) *J. Biol. Chem. 267*, 6502−6509.
14. Gazit, E., and Shai, Y. (1993) *Biochemistry 32*, 12363−12371.
15. Gazit, E., and Shai, Y. (1995) *J. Biol. Chem. 270*, 2571−2578.
16. Rapaport, D., Danin, M., Gazit, E., and Shai, Y. (1992) *Biochemistry 31*, 8868−8875.
17. Ben-Efraim, I., Bach, D., Shai, Y. (1993) *Biochemistry 32*, 2371−2377.
18. Peled, H., and Shai, Y. (1994) *Biochemistry 33*, 211−7219.
19. Ben-Efraim, I., and Shai, Y. (1996) *Protein Sci 5*, 2287−229.
20. Runnels, L. W., and Scarlata, S. F. (1995) *Biophys J 69*, 1569−1583.
21. Erijman, L., and Weber, G. (1991) *Biochemistry 30*, 595−1599.
22. Erijman, L., and Weber, G. (1993) *Photochem Photobiol 57*, 411−415.
23. Hamman, B. D., Oleinikov, A. V., Jokhadze, G. G., Traut, R. R, Jameson, D. M. (1996) *Biochemistry 35*, 16680−16686.
24. Weber, G., and Shinitzky, M. (1970) *Proc. Natl. Acad. Sci. U.S.A. 65*, 823−830.
25. Chattopadhyay, A., and London, E. (1988) *Biochim. Biophys. Acta 938*, 24−34.
26. Arvinte, T., Cudd, A., and Hildenbrand, K.(1986) *Biochim. Biophys. Acta 860*, 215−228.
27. Mazeres, S., Schron, V., Tocanne, J. F., and Lopez, A. (1996) *Biophys. J. 71*, 327−335.
28. Demchenko, A. P. (1986) in *Ultra-violet Spectroscopy of Proteins*, pp 158−192, Springer-Verlag, Berlin, Heidelberg.
29. Ren, J., Lew, S., Wang, Z. and London, E. (1997) *Biochemistry*. 36, 10213−10220
30. Craver, F. W. (1971) *Mol. Phys. 22*, 403−420.
31. Wolber, P. K., and Hudson, B. S. (1979) *Biophys. J.* 28, 197−210.
32. MacPhee, C. E., Perugini, M. A., Sawyer, W. H., and Howlett, G. J. (1997) *FEBS Lett. 416*, 265−268.
33. Byron, O. (1997) *Biophys. J. 72*, 408−415.
34. Schuck, P., MacPhee, C. E., and Howlett, G. J.(1998) *Biophys. J. 74*, 466−474.
35. Palgunachari, M. N., Mishra, V. K., Lund-Katz, S., Phillips, M. C., Adeyeye, S. O., Alluri, S., Anantharamaiah, G. M., and Segrest, J. P. (1996) *Arterioscler Thromb Vasc Biol 16*, 328−338.
36. Lins, L., Brasseur, R., De Pauw, M., Van Biervliet, J. P., Ruysschaert, J. M., Rosseneu, M., and Vanloo, B. (1995) *Biochim Biophys Acta 1258*, 10−18.
37. Sparrow, J. T., Sparrow, D. A., Fernando, G., Culwell, A. R., Kovar M., and Gotto, A. M. (1992) *Biochemistry 31*, 1065−1068.
38. Sparrow, J. T., Sparrow, D. A., Culwell, A. R., and Gotto, A. M. (1985) *Biochemistry 24*, 6984−6988.
39. Lambert, D. A., Catapano, A. L., Smith, L. C., Sparrow, J. T., and Gotto, A. M. (1996) *Atherosclerosis 127*, 205−212.
40. McConathy, W. J., Gesquiere, J. C., Bass, H., Tartar, A., Fruchart, J. C., and Wang, C. S. (1992) *J. Lipid. Res 33*, 995−1003.
41. Catapano, A. L. (1987) *Chem. Phys. Lipids. 45*, 39−47.
42. Wang, C. S., McConathy, W. J., Kloer, H. U., and Alaupovic, P. (1985) *J Clin Invest 75*, 384−390.
43. Matsuoka, N., Shirai, K., and Jackson, R. L. (1980) *Biochim. Biophys. Acta 620*, 308−316.

BI990726B